
LÉVY INDUCED STOCHASTIC DIFFERENTIAL EQUATION EQUIPPED WITH NEURAL NETWORK FOR TIME SERIES FORECASTING

A PREPRINT

Luxuan Yang^a, Ting Gao^a, Yubin Lu^a, Jinqiao Duan^c, and Tao Liu^d

^aSchool of Mathematics and Statistics & Center for Mathematical Sciences, Huazhong University of Science and Technology, Wuhan 430074, China

^cDepartment of Applied Mathematics, College of Computing, Illinois Institute of Technology, Chicago, IL 60616, USA

^dSecurities Finance Department, China Securities Co., Ltd

ABSTRACT

With the fast development of modern deep learning techniques, the study of dynamic systems and neural networks is increasingly benefiting each other in a lot of different ways. Since uncertainties often arise in real world observations, SDEs (stochastic differential equations) come to play an important role. To be more specific, in this paper, we use a collection of SDEs equipped with neural networks to predict long-term trend of noisy time series which has big jump properties and high probability distribution shift. Our contributions are, first, we explored SDEs driven by α -stable Lévy motion to model the time series data and solved the problem through neural network approximation. Second, we theoretically proved the convergence of the model and obtained the convergence rate. Finally, we illustrated our method by applying it to stock marketing time series prediction and found the convergence order of error.

Keywords Stochastic Differential Equations, ResNet and α -stable Lévy motion

Lead Paragraph

Time series analysis with various advanced deep learning mechanisms has been significantly investigated recently. Financial data, especially stock price prediction is considered to be an important task for many quantitative researchers. However, as there always exists various kinds of uncertainties in the forecasting problems, how to accurately capture the intrinsic volatile nature of financial time series data is still challenging. In this paper, we try to improve prediction performance from the viewpoint of stochastic dynamical systems by embedding neural network approximation into the classical numerical SDE (stochastic differential equations) algorithms driven by α -stable Lévy motion. In this way, our method will appropriately capture the uncertainties from both the model and the data, which leads high-accurate prediction results even for data that has distribution discrepancy on training and testing sets. Besides, we also prove the convergence of our network structure, which will facilitate the interdisciplinary study between conventional numerical analysis and deep learning theory.

1 Introduction

Traditional approaches to time series forecasting often have the limitation of assuming that the time series is generated from linear process. However, in most real cases, especially financial stock data, often meets complex nonlinear relationship, even complex chaotic behaviors. Chaotic theory is suitable for nonlinear prediction where phase space reconstruction is one of the most important ideas. Cao [1] proposed a practical method to determine the minimum embedding dimension for a scalar time series. This method only needs one parameter, delay time, and a small amount of data when calculating the embedding dimension. Huang [2] adopted Cao's method for its robust handling of noise

and reconstructed observed financial time series into a high-dimensional phase space. Yu [3] used mutual information to calculate delay interval and Cao’s method to obtain the embedding dimension in order to predict stock prices in reconstructed phase space. Considering the complex non-linear characteristics of stock time series, Zhong [4] improved short-term stock prediction by using PSRT (Phase Space Reconstruction Theory) combined with RNN (Recurrent Neural Network) in which the input dimension of RNN was determined by the minimal embedding dimension. This inspires us that applying phase space reconstruction to chaotic time series data is an appropriate embedding strategy got input representation.

Recently, deep learning models outperform conventional methods in many aspects and has led growing amount of researches to utilize various deep learning framework in the research of time series forecasting. One of the promising models, transformer, is bound to have a prominent prospect. Vaswani [5] conducted experiments in the scenario of machine translation, which completely defeated the State of the Art at the time, and due to the use of parallel computing, the training time has been greatly shortened. Furthermore, many variants of transformer models have emerged in the past two years, such as informer [6] and autoformer [7]. Informer proposes the ProbSparse self-attention mechanism, which reduces the network size and improves long-term sequence prediction. In addition, the long sequence output is obtained through the generative decoder, which avoids the cumulative error propagation in the inference stage. Autoformer also boosts the performance of long-term sequence prediction by using the random process theory, which discards the self-attention mechanism of point-wise connections, and replaces with the autocorrelation mechanism of series-wise connections instead. Moreover, based on the classic method of time series analysis, it designs sequence decomposition units to embed deep models to achieve progressive prediction. Besides making changes to self-attention, adding mathematical theories to the transformer also becomes a popular direction. Macaron Transformer [8] establishes an analogy between the multi-particle dynamic system in physics and the model structure, which benefits the understanding of the intrinsic mechanisms of Transformer.

With the help of mathematical theory, a new class of models emerges. For example, neural network ODE [9] is a combination of residual network and ordinary differential equations. The output of the network is calculated with a black box differential equation solver by adjoint methods. The article also builds a time series signal generation model through the variational autoencoder (VAE) framework, and uses the neural network ODE as a part of it. On the basis of ordinary differential equations, an innovative neural network based on stochastic differential equations, SDE-Net [10] captivates us. The core of the SDE-Net is to treat the deep neural network transformation as the state evolution of a stochastic dynamic system, and introduce the Brownian motion term to capture cognitive uncertainty. In addition, there are also studies using neural networks to solve mathematical problems. The PINNs(Physics-Informed Neural Networks) [11] model just is a combination of mathematics and deep learning. Lu [12] summarizes PINNs(Physics-Informed Neural Networks) and analyzes the feasibility of PINNs to solve partial differential equations. Chen [13] proposes a new framework based on PINNs(Physics-Informed Neural Networks) with a new loss function to solve inverse stochastic problems. Besides, there are even articles that combine finance, mathematics and deep learning. Lukas [14] proves that it is reasonable to use DNN in financial modeling of a large basket in a market with a jump.

Since the neural network is a black box, people hope to explain some of its characteristics through theoretical analysis. Siegel and Xu [15] get the convergence rate of the two-layer neural network under different conditions with the mathematical tools of Fourier analysis. E [16] defines the Barron space and gives direct and inverse approximation theorems holding for functions in the Barron space under two-layer neural network. Li [17] pays attention to the deep residual neural network, which can be regarded as continuous-time dynamical systems and summarized some results on the approximation properties in continuous time.

The rest of this paper is organized as follows. Section 2 introduces our problem and data exploration. We use phase space reconstruction to effectively extract data feature representation by viewing the dynamics of monitoring data. Section 3 presents our neural network model based on stochastic differential equation induced by lévy motion. The theoretical analysis of the model is given in Section 4. In Section 5, experimental results with actual data (financial data) on various tasks are reported, which can help to evaluate the applicability and effectiveness of the model. We conclude the paper and give future research directions in Section 6.

Our main contributions are: First, we design an α -stable Lévy motion induced SDE (stochastic differential equation) to recognize model uncertainty. The experiment results prove that the use of non-Gaussian processes increases the accuracy of model predictions. Second, we combine the convergence of Euler-Maruyama discrete numerical solution with the convergence of the neural network to obtain the new convergence rate of the algorithm. This convergence rate avoids the curse of dimensionality. Third, we bring the attention mechanism into the model so that the proposed LDE-Net can achieve the goal of multi-time step prediction.

To better state our work framework for complex chaotic data prediction, we plot our modeling process in the following flow chart. (Figure 1).

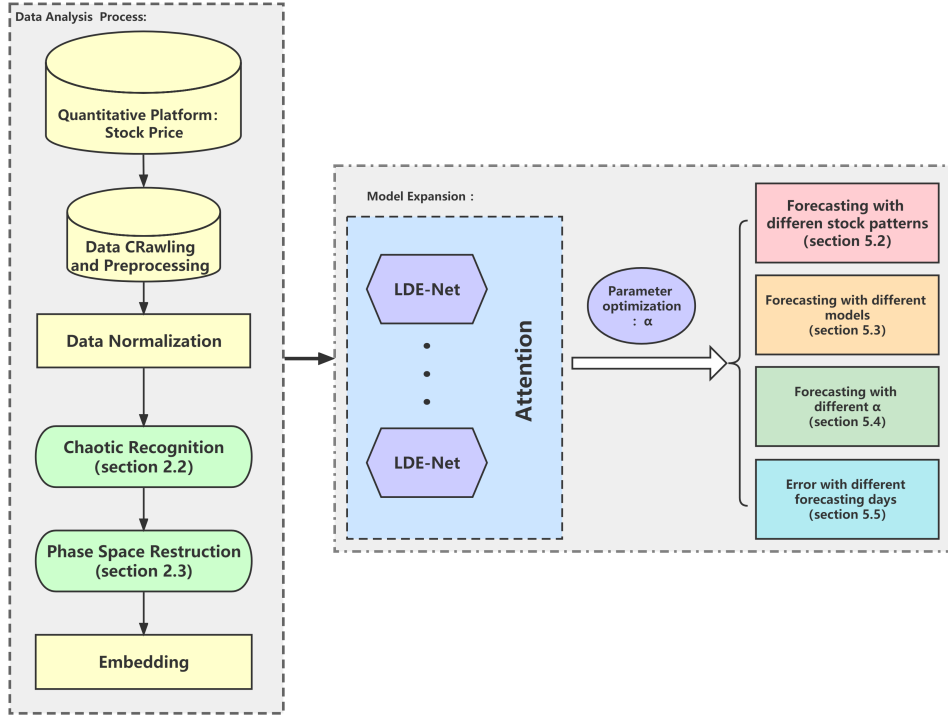


Figure 1: Experiment framework of the stock price series prediction process.

2 Data Exploration and Problem Setting

2.1 Data

Time series in many real scenarios usually appear to be in irregular and hard to understand, so it is important to uncover the governing laws hidden under a non-linear mapping. Chaotic time series can be exactly a type of sequence that restores its original system through mapping.

The financial market is an important part of the economy, which is related to the national economic development and social stability. Financial data, especially stock price, is often viewed as a time series of multiple factors which factors can be divided into two aspects: macro and micro. The macro factors mainly include national policies, economic environment, etc. and the micro factors are mainly market factors, like internal company, industry structure, investor psychology, and so on. As investors' strategies will continue to change along with these factors, the financial market is actually a complex dynamic system. With the liberalization and facilitation of trade and investment policies, financial markets no longer remain linear, but abstract into an extremely complex nonlinear system. Sometimes financial data will even show big jump patterns along with the distribution shift. Due to the non-stationary and non-linearity of the financial market, it is a difficult project to describe it completely so that we can only observe the time series of certain state components in the system. In the past, researchers performed analysis by assuming that the system is stationary and using linearization to eliminate the nonlinear characteristics of the system. But in the face of financial shocks and financial crises, linearization is clearly inexplicable. Then, people discovered that the stock price would change over time and was also affected by the average price volatility, so they tried to simulate it with geometric Brownian motion. The GBM (Geometric Brownian Motion) model incorporates this idea of random walks in stock prices through its uncertain component, along with the idea that stocks maintain price trends over time as the certain component [18]. However, this model is too ideal and may not be suitable for practical situations. Therefore, people gradually began to pay attention to the chaotic characteristics in nonlinear systems. The chaotic theory of nonlinear complex dynamics science holds that: all realistic nonlinear systems are in dynamic evolution, and may present periodic ordered states and non-periodic disordered states (that is, chaotic states) during their evolution; The state of the linear system at a certain moment depends on the value of the state parameter in the system, and changes with the value of the parameter [19]. The emergence of phase space reconstruction methods allows us to identify the chaotic characteristics of the financial system.

2.2 Chaos Recognition

Based on Takens Theorem [20], we know that chaotic time series can restore the original system to establish a prediction model. Therefore, identifying the chaos of time series is the basis of prediction. There are many ways to identify whether a time series is chaotic, such as the largest Lyapunov exponent method, power spectrum method, system phase diagram structure method etc.. Here we use the largest Lyapunov exponent method.

The Lyapunov exponent can describe the characteristics of the dynamics of the system. Assuming if that the value of Lyapunov is represented by λ , we have three cases: (i) $\lambda < 0$, the motion state of the system tends to be stable and is not sensitive to the initial state of the system at this time. (ii) $\lambda = 0$, the system is in a stable state. (iii) $\lambda > 0$, the system movement will enter a chaotic state, and the corresponding mapping is called chaotic mapping. Therefore, judging the magnitude and sign of the Lyapunov exponent becomes a criterion for whether the system enters chaos. The calculation methods of the maximum Lyapunov exponent mainly include definition method, wolf method, orthogonal method and small number method. For unknown nonlinear dynamic systems, we use the wolf method of orbit tracking to solve the maximum Lyapunov exponent of the sequence.

Wolf Method

Since we cannot find the exact differential equation of the original dynamic system, we only calculate the maximum Lyapunov exponent through univariate time series by using analysis and orbit tracking methods. In 1985, Wolf et al. proposed a method to estimate the maximum Lyapunov exponent based on the evolution of phase trajectories, phase planes, and phase volumes. This method is based on orbit tracking which is widely used in the prediction of chaotic time series.

Assuming that the chaotic time series is $x_1, x_2 \dots x_n$, the embedding dimension is m , and the delay time is τ , then the reconstructed phase space is

$$Y(t_i) = (x(t_i), x(t_{i+\tau}), \dots, x(t_{i+(m-1)\tau})), \quad i = 1, 2, \dots, N. \quad (2.1)$$

Taking the initial point as $Y(t_0)$ and the nearest point of it as $Y_0(t_0)$, we define L_0 as the distance between them. Then, we track the evolution of the distance between these two points over time until L_0 reaches the critical value ε ($\varepsilon > 0$) at t_1 , that is $L_1 = |Y(t_1) - Y_0(t_1)| > \varepsilon$. Similarly, we keep $Y(t_1)$ and find its nearest point $Y_1(t_1)$. We set $L'_1 = |Y(t_1) - Y_1(t_1)| < \varepsilon$ and hope that the angle of L_1 and L'_1 is as small as possible. Continue the above process until $Y(t)$ reaches the end of the time series N . The total number of iterations of this process to track the evolution is M . Then, LLE (Largest Lyapunov Exponents) is :

$$\lambda = \frac{1}{t_M - t_0} \sum_{i=1}^M \ln\left(\frac{L'_i}{L_i - 1}\right). \quad (2.2)$$

2.3 Feature Embedding with Phase Space Reconstruction

After judging the chaos, we need to represent our feature embedding. The phase space reconstruction technology has two key parameters: the embedded dimension and the delay time. We assume that the time delay τ is not related to the reconstruction dimension m during reconstruction. Since the current moment is usually related to the information at the previous moment, we choose the time delay $\tau = 1$ to ensure the integrity of the information. The next step is to calculate its embedding dimension.

Due to the fact that the chaotic sequence is actually the result of the trajectory generated by the chaotic system in the high-dimensional phase space being projected into one dimension, this will cause the motion trajectory to be distorted during the projection process. In order to make the information extracted from the low-dimensional data incomplete and accurate, we need to choose the reconstruction dimension to recover the chaotic motion trajectory from the chaotic time series. The usual method of determining the embedding dimension in practical applications is to calculate some geometric invariants of the attractor (such as correlation dimension, Lyapunov exponent, etc.). From the analysis of Takens embedding theorem, it can be seen that these geometric invariants have the geometric properties of attractors. When the dimension is greater than the minimum embedding dimension, the geometric structure has been fully opened. At this time, these geometric invariants have nothing to do with the embedding dimension. Based in this theory, the embedding dimension when the geometric invariant of the attractor stops changing can be selected as the reconstructed phase space dimension.

Cao's Method

In terms of determining the embedding dimension of the phase space, Cao False Nearest Neighbour Method (Cao's Method) [1] is considered to be one of the effective methods to calculate the embedding dimension. There are three advantages of using Cao's method to calculate the embedding dimension: First, it is only necessary to know the delay time parameter in advance. Second, only small amount of data is required. Third, random signals and deterministic signals can both be effectively identified.

Suppose the reconstructed data is:

$$X(t_i) = (x(t_i), x(t_{i+\tau}), \dots, x(t_{i+(m-1)\tau})), i = 1, 2, \dots, N. \quad (2.3)$$

Then the distance $R_{m(i)}$ between it and its nearest neighbor is

$$R_m(i) = \|X_m(i) - X_m^{FNN}(i)\|_2, \quad (2.4)$$

where $X_m^{FNN}(i)$ is the nearest neighbor of $X_m(i)$.

Define

$$a(i, m) = \frac{R_{m+1}(i)}{R_m(i)} = \frac{\|X_{m+1}(i) - X_{m+1}^{FNN}(i)\|}{\|X_m(i) - X_m^{FNN}(i)\|}, \quad (2.5)$$

when $X_{m+1}^{FNN}(i)$ and $X_m^{FNN}(i)$ are close, use the next adjacent point instead [21].

Next, calculate

$$E(m) = \frac{1}{N - m\tau} \sum_{i=1}^{N-m\tau} a(i, m), \quad (2.6)$$

$$E_1(m) = E(m+1)/E(m). \quad (2.7)$$

When the value of m keeps increasing and is greater than a certain value, the amplitude of the change of $E_1(m)$ can be neglected, resulting in saturation. At this time, the corresponding $m+1$ value is the best embedding dimension of the system.

Finally, we have

$$E^*(m) = \frac{1}{N - m\tau} \sum_{i=1}^{N-m\tau} |x_{i+m\tau} - x_{n(i,m)+m\tau}|, \quad (2.8)$$

$$E_2(m) = E^*(m+1)/E^*(m). \quad (2.9)$$

If for any m , $E_2(m) = 1$, it is a random time series, that is, each value of data is independent. If there is always some m , such that $E_2(m) \neq 1$, it is a deterministic time series, that is, the relationship between data points depends on the change of the embedding dimension m .

After calculating the maximum Lyapunov exponent, $E_1(m)$ and $E_2(m)$, we can identify the chaos and predictability of the sequence, and determine the reconstruction dimension. In this way, the dimension of the time series is restored to the original high dimension so that its potentially valuable features are extracted. At the same time, we also get the best input feature embedding for our model.

3 Model

After we determine the input data structure, it is time to build a predictive model for the data. In the earlier days, time series forecasting often used linear autoregression models, such as AR, MA, ARIMA, etc. With the development of machine learning, people began to apply it to prediction such as RNN, LSTM, GRU. Because the structure of neural

network lacks interpretability, people try to seek an explanation from mathematical theory. Until the emergence of residual neural networks (ResNet), people found that it can be viewed from the perspective of differential equations. As we know, ResNet actually corresponds to ordinary differential equations from dynamic system point of view. However, the actual data sometimes produces non-Gaussian fluctuations, which cause the dynamic system to have limitations with uncertainties from the hidden layers. Therefore, we propose a new neural network architecture from the point of view of stochastic differential equations with α -stable Lévy motions. Under this framework, our model can not only estimate the epistemic uncertainty caused by non-Gaussian fluctuations, but also break the traditional single-step prediction of phase space reconstruction technology to achieve multi-step prediction.

3.1 ResNet to Ordinary Differential Equation

As the neural network maps the input x to the output y through a series of hidden layers, the hidden representation can be regarded as the state of a dynamic system [10]. The combination of neural network structure and numerical solution method is becoming more and more popular. Lu et al. [22] confirmed that many neural networks can be interpreted as different numerical discretizations of differential equations. In particular, ResNet can be regarded as a form of Euler discrete solution of ordinary differential equations. Consider the residual network structure Figure 2:

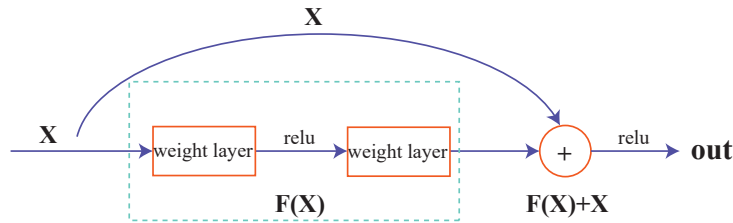


Figure 2: Resnet Structure.

The network can be described by the following equation:

$$\mathbf{x}_{t+1} = \mathbf{x}_t + f(\mathbf{x}_t; \theta), \quad (3.1)$$

where \mathbf{x}_t is the hidden state of the t -th layer. If we let $\Delta t = 1$, the above formula can be written as:

$$\frac{\mathbf{x}_{t+\Delta t} - \mathbf{x}_t}{\Delta t} = f(\mathbf{x}_t; \theta), \quad (3.2)$$

if we let $\Delta t \rightarrow 0$, then there is:

$$\lim_{\Delta t \rightarrow 0} \frac{\mathbf{x}_{t+\Delta t} - \mathbf{x}_t}{\Delta t} = \frac{d\mathbf{x}_t}{dt} = f(\mathbf{x}_t; \theta) \iff d\mathbf{x}_t = f(\mathbf{x}_t; \theta) dt. \quad (3.3)$$

From the above reasoning process, we can see that ResNet can indeed match the Euler discretization of ordinary differential equations very well. For each hidden layer of the neural network, the motion process of the input value in it is actually an iterative formula of the Euler method. This analogy can effectively help us understand the inner behavior of ResNet. Based on this research direction, Chen et al. [9] used the ODE Solver to transform the discretized Euler method into a continuous form so that the parameters became a continuous space without the need to propagate gradients and update parameters in layers.

3.2 Differential Equation under α -stable Lévy Motion

Neural ODEs (Ordinary Differential Equations) explain the state of the hidden layer through a deterministic dynamic system. Although this way is clever, it cannot capture the potential uncertainty caused by the model. In fact, this ability is essential for tasks that value risk. Therefore, It is necessary for us to quantify uncertainties. Kong et al.'s [10] research shows that the uncertainty of model prediction comes from two aspects: (1) aleatoric uncertainty: it comes from the natural randomness in the task itself (such as label noise, etc.) (2) epistemic uncertainty: due to lack of training data, the model's estimate of the input data is inaccurate. For aleatory uncertainty, it is naturally determined by the task itself. You can imagine a training set in which all labels are noisy. A model trained with such a data set will

obviously have unreliable prediction results, that is, the uncertainty is very high. For epistemic uncertainty, it is caused by insufficient cognition of the model. When faced with poor training and insufficient training data, the prediction result of the model will have a higher degree of uncertainty.

In order to model epistemic uncertainty, Kong et al. [10] used the stochastic differential equation with Brownian motion to replace the original hidden layer structure of ResNet, so that the deterministic dynamic system became stochastic. However, this dynamic fluctuation in the hidden layers does not necessarily satisfy Gaussian. There may be a big jump or distribution shift in trend of data, especially for actual data. In this case, using Brownian motion to capture epistemic uncertainty, the optimized parameters may not be optimal. Hence, we hope to use non-Gaussian noise to improve the universality of predictive model. We propose LDE-Net model whose core is to capture cognitive uncertainty through α -stable Lévy motion.

Lévy Motion Let $X = (X(t), t \geq 0)$ be a stochastic process defined on a probability space (Ω, \mathcal{F}, P) . We say that X is a Lévy motion if: (L1) $X(0) = 0$ (a.s.); (L2) X has independent and stationary increments; (L3) X is stochastically continuous, i.e. for all $a > 0$ and for all $s \geq 0$, $\lim_{t \rightarrow s} P(|X(t) - X(s)| > a) = 0$, for all $a > 0$.

Symmetric α -Stable Random Variables $X \sim S_\alpha(\sigma, \beta, \gamma)$ is called a symmetric α -stable random variable if $\beta = 0$ and $\gamma = 0$, that is, $X \sim S_\alpha(\sigma, 0, 0)$. When $\sigma = 1$, it is called a standard symmetric α -stable random variable, and we denote this by $X \sim S_\alpha(1, 0, 0)$.

Symmetric α -Stable Lévy Motions A symmetric α -stable scalar Lévy motion L_t^α , with $0 < \alpha < 2$, is a stochastic process with the following properties: (i) $L_0^\alpha = 0$, a.s. (ii) L_t^α has independent increments. (iii) $L_t^\alpha - L_s^\alpha \sim S_\alpha\left((t-s)^{\frac{1}{\alpha}}, 0, 0\right)$. (iv) L_t^α has stochastically continuous sample paths, that is, for every $s > 0$, $L_t^\alpha \rightarrow L_s^\alpha$ in probability, as $t \rightarrow s$.

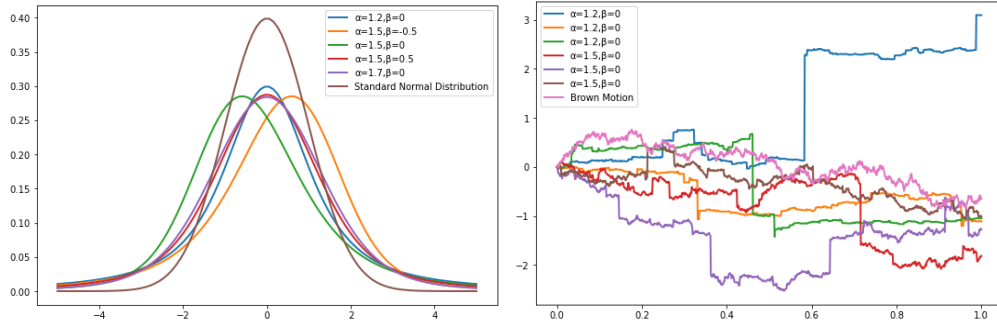


Figure 3: left: Probability distribution functions of standard normal distribution and Lévy motion with different α and β . right: Brownian motion and Lévy motion with different α and β

We add Lévy motion to the right side of Eq.(3.1) to make it the Euler discretization form of the stochastic differential equation. The continuous-time dynamics of the system (3.3) are then expressed as:

$$dx_t = f(x_t; \theta) dt + g(x_t; \theta) dL_t^\alpha. \quad (3.4)$$

The diffusion net g denotes the noise intensity of the Lévy motion. The drift net f in LDE-Net aims to control the system to achieve good predictive accuracy and to capture aleatoric uncertainty. The diffusion network g in LDE-Net represents the epistemic uncertainty for the dynamical system. Like Kong et al. [10], the diffusion of the system also should meet the following conditions: (1) For the region in the training distribution, the noise intensity of the Lévy motion should be small (low diffusion). The system state is dominated by the drift term in this area, and the output noise intensity should be small; (2) For the area outside the training distribution, the noise intensity of the Lévy motion should be large (high diffusion).

3.3 LDE-Net

Since our goal is to capture the uncertainty of the model through stochastic differential equations, we use the form of the numerical solution of the differential equation as the structure of the neural network. So far, there are many kinds

of numerical solutions of differential equations, which can be divided into high-order and first-order according to the expansion order of the equation. Considering that higher-order numerical methods will increase the computational cost and complicate the input structure, we use a simple Euler-Maruyama scheme with a fixed step size for efficient network training.

Besides, we find from SDE-Net [10] that the idea of attack is helpful for parameter optimization. We also added noise to obtain the out-of-distribution (OOD) data which helps to optimize the parameters of the diffusion term, that is, $\tilde{\mathbf{x}}_0 = \mathbf{x}_0 + noise$. Since the traditional phase space reconstruction technology and SDE-Net [10] can only perform single-step prediction, we use the attention mechanism to make the proposed model perform multi-step prediction in parallel. The training process of our proposed model is as follows:

$$\mathbf{x}_{k+1} = \mathbf{x}_k + \underbrace{f(\mathbf{x}_k; \theta_f)}_{\text{drift neural net}} \Delta t + \underbrace{g(\mathbf{x}_k; \theta_g)}_{\text{diffusion neural net}} (\Delta t)^{1/\alpha} L_k, \quad k = 0, 1, \dots, N-1, \quad (3.5)$$

$$\min_{\theta_f} E_{\mathbf{x}_0 \sim P_{train}} E \left(\sum_{i=1}^l L_i(\mathbf{x}_N) \right) + \min_{\theta_g} E_{\mathbf{x}_0 \sim P_{train}} g(\mathbf{x}_0; \theta_g) + \max_{\theta_g} E_{\tilde{\mathbf{x}}_0 \sim P_{OOD}} g(\tilde{\mathbf{x}}_0; \theta_g) \quad (3.6)$$

Here $L_k \sim S_\alpha(1, 0, 0)$ are standard rotationally symmetric α -stable random variables. We use T to denote the terminal time of the random walk of the data in the model and l to represent the forecast days. Then, the time interval $[0, T]$ is divided into N sub-intervals and we get $\Delta t = \frac{T}{N}$. Besides, we define $L_i(\cdot)$ as the loss function on the i -th day during the forecasting process. The symbol P_{train} represents the distribution for training data, and P_{OOD} is the out of distribution data.

The diffusion term will capture epistemic uncertainty caused by big jumps in the data trend. The drift term captures the aleatoric uncertainty by outputting a probability distribution form and controls the prediction accuracy of the system to make the prediction results effective. In addition, the number of steps to solve the SDE can be equal to the number of layers in the traditional neural network definition. In the process of moving through the hidden layer, each of our network layers share the same parameters. And to reduce the computational burden, our diffusion term is only determined by the initial value x_0 . The structure of LDE-Net model is shown in Figure 4.

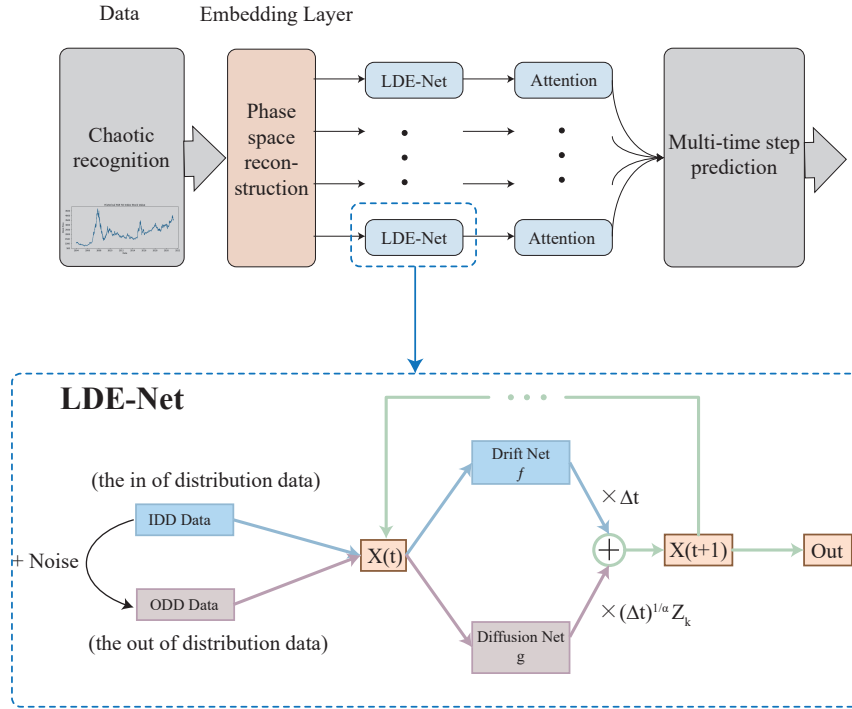


Figure 4: Structure of LDE-Net.

4 Theoretical Analysis

4.1 Theoretical Analysis

In this subsection, we will prove the theoretical results of our LDE-Net model. First of all, we ensure the existence and uniqueness of the solution X_t to a stochastic differential equation with α -stable Lévy motion in the following theorem.

Notice : Theorem 4.1 ensure the existence and uniqueness of the solution X_t to a stochastic differential equation with α -stable Lévy motion so that we can design an effective network architecture. Then, under the assumption H1, we can get the lemma 4.2 so that we gain the strong convergence rate of Euler-Maruyama method for stochastic differential equation with Lipschitz continuous drift coefficient by α -stable motion. Since the numerical solution obtained by Euler-Maruyama method contains hyperparameters of the neural network, we hope to prove that the algorithm converges to a solution without hyperparameters. Under lemma 4.3, we know that any function in Barron space can be approximated by a two-layer neural network. Therefore, we can propose assumption H2 base on lemma 4.3. Then, from Lemma 4.4, we can explain that the solution of the approximate stochastic differential equation with hyperparameters obtained by Euler-Maruyama method can approximate the solution of a potential stochastic differential equation without hyperparameters. Finally, by Lemma 4.2 and Lemma 4.4, we can get Theorem 4.5 which shows the convergence rate of our LDE-Net model.

Theorem 4.1. *Let $\{U, \mathcal{B}_U\}$ be a measurable space and $\nu(du)$ be a σ -finite measure on it. Let U_0 be a set in \mathcal{B}_U such that $\nu(U \setminus U_0) < \infty$. If functions $f(x; \theta_f)$ and $g(x, \theta_g)$ satisfy the Lipschitz condition for every parameter θ_f and θ_g respectively:*

$$\|f(x; \theta_f) - f(y; \theta_f)\|^2 + \int_{U_0} \|g(x; \theta_g)z - g(y; \theta_g)z\|^2 \nu(dz) \leq K|x - y|^2, \quad x, y \in \mathbb{R}^d,$$

there exists a unique (\mathcal{F}_t) -adapted right-continuous process $X(t)$ with left limits which satisfies equation

$$X_t = X_0 + \int_0^t f(X_s; \theta_f) ds + \int_0^t \int_{\mathbb{R} \setminus \{0\}} g(X_s; \theta_g) z \tilde{N}(ds, dz).$$

Here \tilde{N} stands for the compensated Poisson measure. The measure ν is the Lévy measure of random poisson measure N .

The proof of Theorem 4.1 can be found in Duan [23] and Ikeda and Watanabe [24].

Next, we will show the approximation rate of our model with respect to the number of neurons in the hidden layer. The proof is based on the methods used in Zhang [25] and E [16]. We rewrite equation (3.5) in the following form:

$$X_{k+1}^{(m)} = X_k^{(m)} + f_m(X_k^{(m)}; \theta_f) \Delta t + g_m(X_k^{(m)}; \theta_g) (\Delta t)^{1/\alpha} L_k. \quad (4.1)$$

Then, the continuous-time dynamic of the system (3.4) can be correspondingly expressed as:

$$dx_t^{(m)} = f_m(x_t^{(m)}; \theta_f) dt + g_m(x_t^{(m)}; \theta_g) dL_t^\alpha. \quad (4.2)$$

Let m be the number of neurons in the hidden layer and T be the terminal time. Then, we have time step $\Delta t \in (0, 1)$ so that $N = \frac{T}{\Delta t}$. We use \mathcal{B} and $\|\cdot\|_{\mathcal{B}}$ to denote the Barron space and Barron norm. Simultaneously, the superscript (m) of $X^{(m)}$ and $x^{(m)}$ represents them obtained by neural network training. The subscript m of f_m and g_m also have the same meaning.

Assumption H1. Assume that there exists a constant $K > 0$ such that

$$|f_m(x; \theta_f) - f_m(y; \theta_f)| \leq K|x - y|,$$

for any $x, y \in \mathbb{R}^d$ and $m \in \mathbb{N}^+$.

In order to facilitate subsequent proofs, we use $f_m(x)$ to represent $f_m(x; \theta_f)$. Similarly, we use $g_m(x)$ to represent $g_m(x; \theta_g)$. According to Liu [26], we can get Theorem 4.2 under Assumption H1.

Lemma 4.2. *Suppose that Assumption H1 holds, we have the error of the Euler-Maruyama method (4.1) as follows.*

$$\sup_{0 \leq t \leq T} \mathbb{E}|X_k^{(m)}(t) - x^{(m)}(t)| \leq (\Delta t)^{\frac{1}{\alpha}} K C_6 T \exp(KT),$$

where $C_6 = 4K_1(1 + C_5) + 2|g_m(x_0)|C_3$, $C_5 = C_4 + e^{6K_1T}$, $C_4 = 3(\mathbb{E}|x_0| + 2K_1T + C_3T^{\frac{1}{\alpha}}|g_m(x_0)|)$, $K_1 = \max(K, f_m(x_0))$ and C_3 is a constant dependent on α (see the exact expression of C_3 in [27]).

Lemma 4.3. For every $f \in \mathcal{B}$ and constant $m > 0$, there exists a two-layer neural network $f_m(\cdot; \Theta)$, $f_m(\mathbf{x}; \Theta) = \frac{1}{m} \sum_{k=1}^m a_k \sigma(b_k^T \mathbf{x} + c_k)$ (Θ denotes the parameters $\{a_k, b_k, c_k, k \in [m]\}$ in the neural network), such that

$$\|f(\cdot) - f_m(\cdot; \Theta)\|_{L^2}^2 \leq \frac{3\|f\|_{\mathcal{B}}^2}{m},$$

Furthermore, we have

$$\|\Theta\|_{\mathcal{P}} := \frac{1}{m} \sum_{j=1}^m |a_j| (\|b_j\|_1 + |c_j|) \leq 2\|f\|_{\mathcal{B}}$$

The proof of Lemma 4.3 can be found in E [16].

Assumption H2. Assume that there is an underlying SDE:

$$Y(t) = Y(0) + \int_0^t f(Y(s))ds + gL_t, \quad Y(0) = x_0,$$

where L_t is a bounded Lévy motion. Function f is Lipschitz continuous with Lipschitz constant L and bounded.

In our model, two-layer neural networks are used to approximate function f and constant g in the following sense:

$$\|f_m - f\|_{L^2} \lesssim \frac{\|f\|_{\mathcal{B}}^2}{m^{\frac{1}{2}}} \leq C_1 m^{-\frac{1}{2}}, \quad |g_m - g| \leq C_2 m^{-\frac{1}{2}}. \quad (4.3)$$

Here, m is the number of neurons in the hidden layers. f_m and g_m represent the function f and g learned by neural networks. Besides, C_1 and C_2 are constants.

Lemma 4.4. For the approximating SDE:

$$x^{(m)}(t) = x^{(m)}(0) + \int_0^t f_m(X^{(m)}(s))ds + g_m L_t, \quad X(0) = x_0, \quad (4.4)$$

let $u_t^{(m)}$ be the probability density function of $X^{(m)}(t)$. Assume $u_t^{(m)}$ to be uniformly bounded:

$$\sup_{t \in [0, T]} \sup_{x \in \mathbb{R}^d} |u_t^{(m)}(x)| \leq M.$$

Then,

$$\mathbb{E} \left(\sup_{t \in [0, T]} |x^{(m)}(t) - Y(t)| \right) < \tilde{C}(T) m^{-\frac{1}{2}}.$$

Theorem 4.5. Under Assumptions H1 and H2, we have the convergence rate of our LDE-Net model:

$$\sup_{0 \leq t \leq T} \mathbb{E} |X_k^{(m)}(t) - Y(t)| \leq \frac{\tilde{C}(T)}{m^{\frac{1}{2}}} + (\Delta t)^{\frac{1}{\alpha}} K C_6 T \exp(KT),$$

where constants $\tilde{C}(T) = (M^{\frac{1}{2}} T C_1 + C C_2) \exp(LT)$, $C_6 = 4K_1(1 + C_5) + 2|g_m(x_0)|C_3$, $C_5 = C_4 + e^{6K_1 T}$, $C_4 = 3(\mathbb{E}|x_0| + 2K_1 T + C_3 T^{\frac{1}{\alpha}} |g_m(x_0)|)$, $K_1 = \max(K, f_m(x_0))$, constant C is the bound of $|L_t|$ and C_3 is a constant dependent on α (see the exact expression of C_3 in [27]).

The proofs of Lemma 4.2, Lemma 4.4 and Theorem 4.5 are provided in Appendix B.

5 Experiments

In this section, we bring the actual finance data into LDE-Net model for prediction and evaluate the model from three experiments: (1) Identify the data types applicable to the model. (2) Compare the prediction effect with common prediction models for stocks and the SDE neural network with Brown motion. (3) Observe the multi-step prediction results of different α values in Lévy motion. (4) Analyze the effect of forecasting days on prediction accuracy.

5.1 Dataset

We consider different types of stock data and divide them separately into a training set and a testing set according to the ratio of 4 : 1. Then we use the wolf method to calculate the maximum Lyapunov exponent of data, and judge the data as a chaotic time series. Next we calculate the best embedding dimension of the stock data and reconstruct the state space with the Cao's method. Finally, we use the reconstructed data as the input of the LDE-Net model and perform a multi-step prediction, that is, use the data of the previous M (the best embedding dimension) days to predict the data of the next four days. In addition, we compare our proposed model with different models, and consider the impact of different α on data prediction.

Three Types of stock Patterns

According to the different fluctuations of data sets, we select three stocks corresponding to SSE Energy Index, SSE50 Index and SSE Consumer Index. For SSE Energy Index stock, it fluctuates greatly on the training set, but behaves relatively smoothly on the testing set. For SSE50 Index stock, it shows large fluctuations on the training set and relatively small on the testing set. For SSE Consumer Index stock, it performs relatively smoothly on the training set, but fluctuates greatly on the testing set. Furthermore, we select SSE Energy index with a total sample of 3086, SSE50 Index with a total sample of 4194 and SSE Consumer Index with a total sample of 2497 separately from 2009-2021, 2004-2021, and 2011-2021. (See Figure 5)

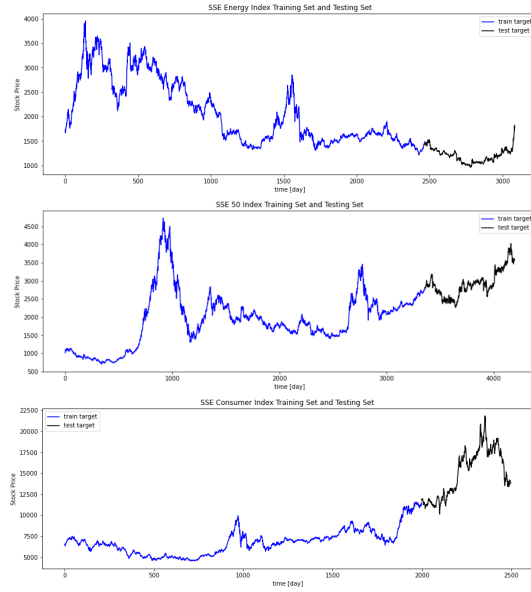


Figure 5: Top: Data set of SSE Energy index. Middle: Data set of SSE 50 index. Bottom: Data set of SSE Consumer Index.

Chaotic Recognition

After completing stock selection, we need to determine the input structure. This requires the use of the phase space reconstruction technique we mentioned earlier. According to the calculation formula of the largest Lyapunov index, we obtain that the three stocks are all chaotic time series. Simultaneously, through the Cao's method for numerical calculation, we determine that their optimal embedding dimensions are: $m_1 = 20$, $m_2 = 23$, $m_3 = 15$. Based on the above results, we obtain the input structure.

Table 1: The Maximum Lyapunov Exponent

Data Set	The Maximum Lyapunov Exponent	Result
SSE Energy Index	0.0254	Chaotic
SSE50 Index	0.0242	Chaotic
SSE Consumer Index	0.0347	Chaotic

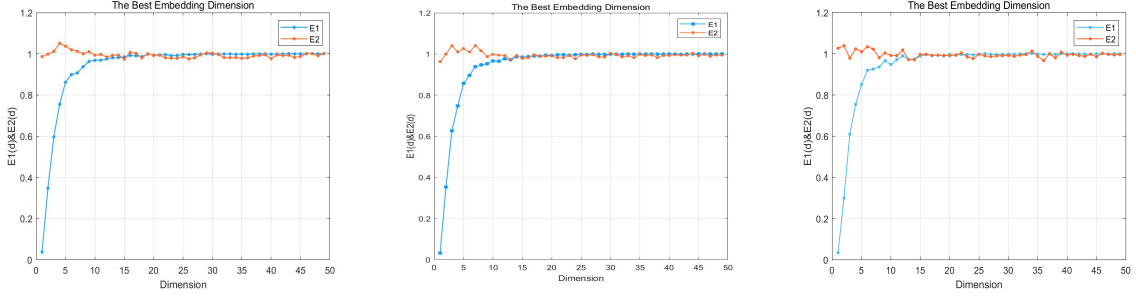


Figure 6: The Best Embedding Dimensions. (left: SSE energy Index stock, middle: SSE50 Index stock, right: SSE Consumer Index stock)

5.2 Experiment 1: Forecasting with different stock patterns

When comparing different stock trend types, we only consider the forecast effect of the fourth day under the same $\alpha = 1.5$. By observing the results of loss, we can determine which type of stock data our model is more suitable for. Here we mainly observe the prediction effect of the fourth day for judgment.

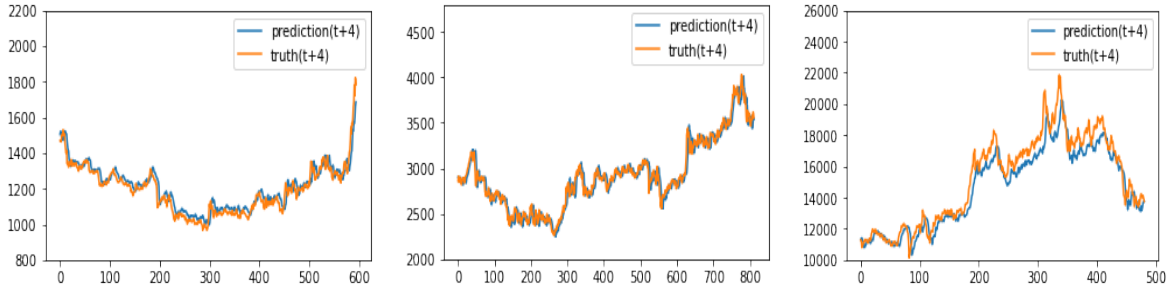


Figure 7: The prediction effect of different stocks on the fourth day. (left:SSE energy Index stock, middle: SSE50 Index stock, right: SSE Consumer Index stock)

Table 2: Forecast results of different stock ($\alpha = 1.5$)

Data	MSE(t+1)	MSE(t+2)	MSE(t+3)	MSE(t+4)
SSE energy Index	0.0010	0.0022	0.0034	0.0045
SSE50 Index	0.0029	0.0058	0.0091	0.0125
SSE Consumer Index	0.2024	0.2210	0.1951	0.3301

As can be seen from the Figure 7, the prediction effect of SSE Consumer Index Stock is the worst and the LDE-Net model is suitable for predicting the future value of stocks with large fluctuations in historical data. When the training set fluctuates more frequently with larger amplitude, Lévy noise can better capture the uncertainty in the prediction process, so as to achieve more accurate prediction. However, historical data in Consumer Index Stock is flatten while prediction set has bigger volatility, which is just the opposite of the trend situation described earlier. Therefore, the fitting effect between the predicted result and the true value is not ideal for Consumer Index Stock. In the follow-up part, we will choose SSE Energy Index Stock and SSE50 Index Stock for experimentation to confirm the significance of LDE-Net.

5.3 Experiment 2: Forecasting with different models

Under the condition of setting $\alpha = 1$, we compare the proposed model with the traditional SDE-Net [10] and commonly used forecasting models for stock data to check whether the proposed model makes sense. We have chosen LSTM [28] and ARIMA [29], for common models. Since the accuracy of forecasting one day is the highest, we only

compare the effect of forecasting one day. Here we only show the prediction effect images of SSE energy Index stock with same coordinate scales.

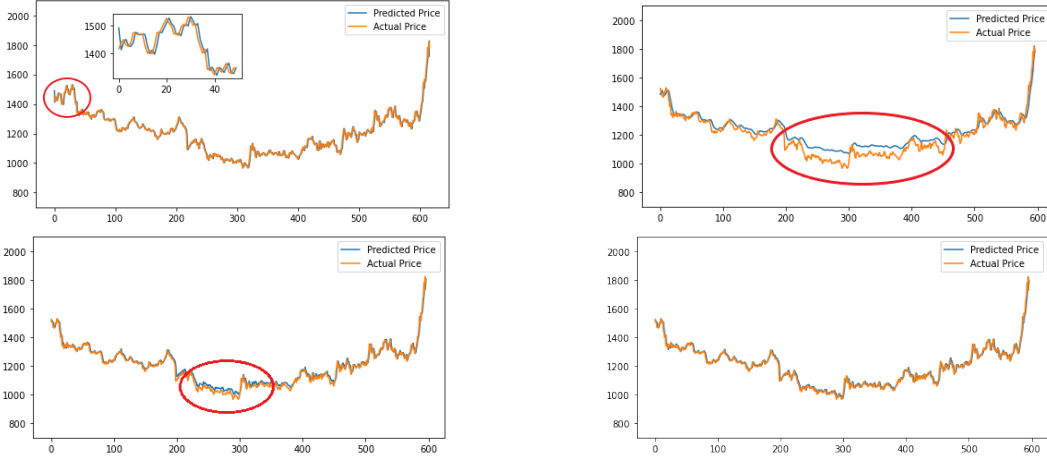


Figure 8: For SSE energy Index stock, the predictive effects of different models. (The upper left is ARIMA, the upper right is LSTM, the lower left is SDE-Net, the lower right is LDE-Net.)

From the above figures (Figure 8) only for SSE energy Index stock, we can intuitively find that the prediction effect of LDE-Net is the best. The predicted values of LSTM and SDE-Net in the next 200-300 days (testing set) are obviously not close to the true values. Although the predicted values of ARIMA seem to fit very well overall, it can be seen that the first few real values are not close to the predicted values. We select the first 50 data of the testing set and refine the coordinate scale to zoom in and observe the prediction effect. It can be found that the curve fitted by ARIMA has a significant time lag. Therefore, ARIMA seems to be accurate on the surface, but it is actually a visual error caused by the large coordinate scale. In order to see the difference more specifically, we give a comparison table of loss defined by MSE, RMSE and MAE for SSE energy Index stock and SSE 50 Index stock.

Table 3: Forecast results of different models

Data	Model	MSE	RMSE	MAE
SSE energy Index	ARIMA	0.0188	0.1371	0.0945
	LSTM	0.0054	0.0735	0.0597
	SDE-Net	0.0011	0.0335	0.0256
	LDE-Net	0.0009	0.0295	0.0209
SSE 50 Index	ARIMA	0.0113	0.1064	0.0767
	LSTM	0.0031	0.0554	0.0408
	SDE-Net	0.0030	0.0546	0.0394
	LDE-Net	0.0029	0.0537	0.0386

From the three indicators in the Table 3, it is verified that the conclusions we have obtained based on the images are correct. For the two types of stock representative data, the prediction effect of our LDE-Net is better than other models. For SSE Energy Index Stock, the MSE value is about 0.08672%, and the accuracy is 29% higher than the original SED-Net. In addition, RMSE is about 2.945%, and the error is 0.401% less than SED-Net. Also, MAE is reduced by about 0.47%. For SSE 50 Index Stock, the values of RMSE and MAE is about 0.1% less than SED-Net. In general, the proposal of LDE-Net has a certain meaning.

5.4 Experiment 3: Forecasting with different α

Considering that different α will produce different jumps, we want to observe the effect of model predictive ability without a fixed $\alpha=1.5$. Therefore, we input the reconstructed data into the LDE-Net model with $\alpha = 1.2, 1.3, 1.4, 1.5, 1.6, 1.8$ for the same stock.

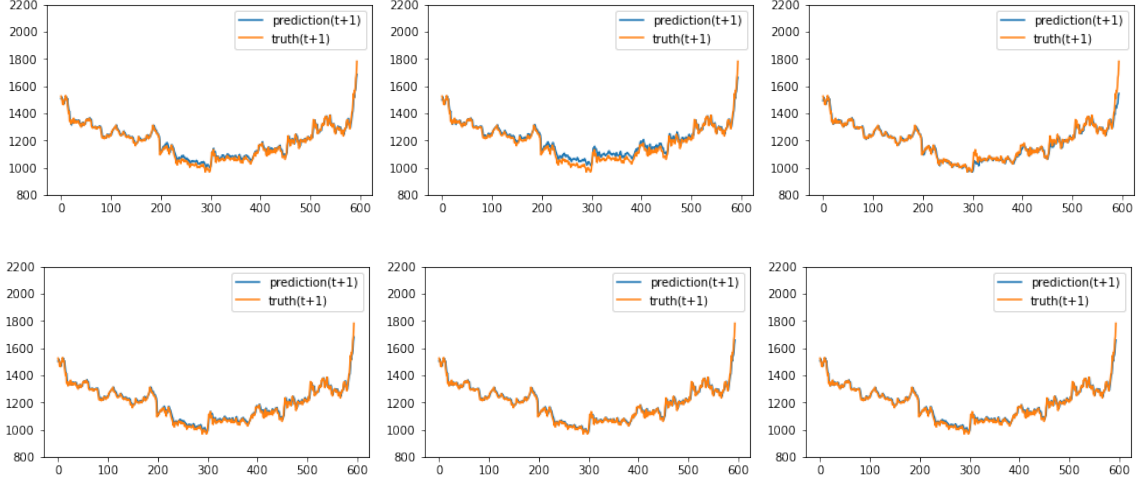


Figure 9: For SSE energy index stocks, the predictive effect of different α . (The upper left is $\alpha = 1.2$, the upper middle is $\alpha = 1.3$, the upper right is $\alpha = 1.4$, the lower left is $\alpha = 1.5$, the lower middle is $\alpha = 1.6$, and the lower right is $\alpha = 1.8$)

Table 4: Forecast results of different α

Data	Value of α	MSE(t+1)1.0*1e-3	MSE(t+2)1.0*1e-3	MSE(t+3)1.0*1e-3	MSE(t+4)1.0*1e-3
SSE energy Index	$\alpha = 1.2$	1.1555	2.8272	3.9941	5.2052
	$\alpha = 1.3$	2.0929	2.2900	4.1513	5.3823
	$\alpha = 1.4$	1.7146	2.4714	3.1843	4.6635
	$\alpha = 1.5$	1.0317	2.2017	3.3650	4.5471
	$\alpha = 1.6$	0.9455	2.1151	2.8728	5.4028
	$\alpha = 1.8$	0.9890	2.0429	2.8211	5.5467
SSE50 Index	$\alpha = 1.2$	3.2909	6.2504	9.3327	13.3091
	$\alpha = 1.3$	3.1861	6.0212	9.6572	12.8533
	$\alpha = 1.4$	2.9535	5.9002	9.4551	12.8543
	$\alpha = 1.5$	2.9415	5.8059	9.1026	12.4943
	$\alpha = 1.6$	2.9809	6.0121	9.6383	12.8007
	$\alpha = 1.8$	2.9804	6.0358	9.4742	12.6342

From the results of the MSE value in the Table 4, it can be seen that the value of α can have a certain influence on the prediction of the model. For example, for the same stock, it can be seen that the best α of SSE Energy Index stock is 1.6, while the best α of SSE 50 Index stock is 1.5. For different stocks, the greater the data fluctuation, the smaller α value of the stock, which is in line with the nature of Lévy motion that is smaller α can give greater jump.

5.5 Experiment 4: Effect of forecasting days on prediction accuracy

We also investigate the order of accuracy over predicting days and get some interesting results. For example, the error is roughly proportional to the length of forecasting days, even if we change the value of α . This linear relationship indicates the the error rate is of $O(1)$.

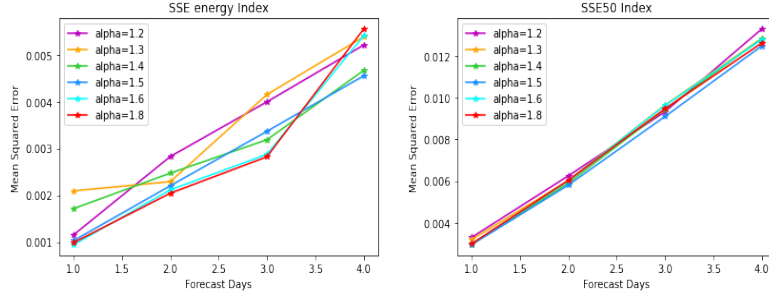


Figure 10: The prediction error rate over forecasting days. (left:SSE energy Index stock, right: SSE50 Index stock)

6 Conclusions

We presented an latent SDE (stochastic differential equation) model equipped with neural networks to forecast financial time series data, which is non-stationary with noise. The whole paper is divided into three parts: data processing, model establishment, theoretical analysis and prediction evaluation. Throughout the experiment, we input the reconstructed data into a neural network that uses α -stable Lévy motion to capture epistemic uncertainty. Moreover, we use the attention mechanism to perform parallel operations on multiple LDE-Nets to achieve multi-day forecasting.

All in all, we conclude our main findings in the following: First, LDE-Net is more suitable for predicting stocks that fluctuate with high volatility, as α -stable Lévy motion can better capture the training data trend with epistemic jumps. Second, We have theoretically proved the convergence of our algorithm. Finally, we also illustrated that the order of accuracy linearly changes over forecast days. For the future research work, one aspect can be optimizing the selection of α values and another direction is to estimate generalization error bound in terms of data complexity.

7 Acknowledge

This work was supported by Fundamental research funds for central universities 5003011053. We would like to thank Wei Wei, Ao Zhang and Huifang Huang for helpful discussion.

References

- [1] Liangyue Cao. Practical method for determining the minimum embedding dimension of a scalar time series. *Physica D: Nonlinear Phenomena*, 110:43–50, 1997.
- [2] Yan Huang, Gang Kou, and Yi Peng. Nonlinear manifold learning for early warnings in financial markets. *Eur. J. Oper. Res.*, 258:692–702, 2017.
- [3] Pengfei Yu and Xuesong Yan. Stock price prediction based on deep neural networks. *Neural Computing and Applications*, 32:1609–1628, 2019.
- [4] Tanwei Zhong. New approach of short-term stock prediction based on combination of phase space reconstruction theory and recurrent neural network. *Application Research of Computers*, 2007.
- [5] Ashish Vaswani, Noam M. Shazeer, Niki Parmar, Jakob Uszkoreit, Llion Jones, Aidan N. Gomez, Lukasz Kaiser, and Illia Polosukhin. Attention is all you need. *ArXiv*, abs/1706.03762, 2017.
- [6] Haoyi Zhou, Shanghang Zhang, Jieqi Peng, Shuai Zhang, Jianxin Li, Hui Xiong, and Wancai Zhang. Informer: Beyond efficient transformer for long sequence time-series forecasting. In *AAAI*, 2021.
- [7] Haixu Wu, Jiehui Xu, Jianmin Wang, and Mingsheng Long. Autoformer: Decomposition transformers with auto-correlation for long-term series forecasting. *ArXiv*, abs/2106.13008, 2021.
- [8] Yiping Lu, Zhuohan Li, Di He, Zhiqing Sun, Bin Dong, Tao Qin, Liwei Wang, and Tie-Yan Liu. Understanding and improving transformer from a multi-particle dynamic system point of view. *ArXiv*, abs/1906.02762, 2019.
- [9] Tianqi Chen, Yulia Rubanova, Jesse Bettencourt, and David Kristjanson Duvenaud. Neural ordinary differential equations. In *NeurIPS*, 2018.
- [10] Lingkai Kong, Jimeng Sun, and Chao Zhang. Sde-net: Equipping deep neural networks with uncertainty estimates. *ArXiv*, abs/2008.10546, 2020.

-
- [11] Maziar Raissi, Paris Perdikaris, and George E Karniadakis. Physics-informed neural networks: A deep learning framework for solving forward and inverse problems involving nonlinear partial differential equations. *Journal of Computational Physics*, 378:686–707, 2019.
- [12] Lu Lu, Xuhui Meng, Zhiping Mao, and George Em Karniadakis. Deepxde: A deep learning library for solving differential equations. *SIAM Review*, 63(1):208–228, 2021.
- [13] Xiaoli Chen, Liu Yang, Jinqiao Duan, and George Em Karniadakis. Solving inverse stochastic problems from discrete particle observations using the fokker–planck equation and physics-informed neural networks. *SIAM Journal on Scientific Computing*, 43(3):B811–B830, 2021.
- [14] Lukas Gonon and Christoph Schwab. Deep relu network expression rates for option prices in high-dimensional, exponential Levy models. *arXiv preprint arXiv:2101.11897*, 2021.
- [15] Jonathan W Siegel and Jinchao Xu. Approximation rates for neural networks with general activation functions. *Neural Networks*, 128:313–321, 2020.
- [16] Weinan E, Chao Ma, and Lei Wu. The barron space and the flow-induced function spaces for neural network models. *Constructive Approximation*, pages 1–38, 2021.
- [17] Qianxiao Li, Ting Lin, and Zuwei Shen. Deep learning via dynamical systems: An approximation perspective. *arXiv preprint arXiv:1912.10382*, 2019.
- [18] Krishna Reddy and Vaughan Clinton. Simulating stock prices using geometric brownian motion: Evidence from australian companies. *The Australasian Accounting Business and Finance Journal*, 10:23–47, 2016.
- [19] Jun Ma, Yinshuo Zhang, and Zhanhui Cao. Chaos characteristics of space object res based on cao method. *Modern Radar*, 2009.
- [20] Floris Takens. Detecting strange attractors in turbulence. In David Rand and Lai-Sang Young, editors, *Dynamical Systems and Turbulence, Warwick 1980*, pages 366–381, Berlin, Heidelberg, 1981. Springer Berlin Heidelberg.
- [21] Lihua Li. The research of financial chaos based on phase space reconstruction technology. *Hunan University of Arts and Science (in Chinese)*, 2011.
- [22] Yiping Lu, Aoxiao Zhong, Quanzheng Li, and Bin Dong. Beyond finite layer neural networks: Bridging deep architectures and numerical differential equations, 2020.
- [23] Jinqiao Duan. *An Introduction to Stochastic Dynamics*. Cambridge Texts in Applied Mathematics. Cambridge University Press, 2015.
- [24] Nobuyuki Ikeda and Shinzo Watanabe. *Stochastic Differential Equations and Diffusion Processes*. Kodansha scientific books. North-Holland, 1989.
- [25] Ao Zhang and Jinqiao Duan. Kantorovich–rubinstein distance and approximation for non-local fokker–planck equations. *Chaos: An Interdisciplinary Journal of Nonlinear Science*, 31(11):111104, 2021.
- [26] Wei Liu. Strong convergence rate of euler-maruyama method for stochastic differential equations with hölder continuous drift coefficient driven by symmetric α -stable process. *arXiv preprint arXiv:1901.08742*, 2019.
- [27] Gennady Samorodnitsky and Murad S. Taqqu. Stable non-gaussian random processes : Stochastic models with infinite variance. *Journal of the American Statistical Association*, 90:805, 1995.
- [28] Sepp Hochreiter and Jürgen Schmidhuber. Long short-term memory. *Neural computation*, 9(8):1735–1780, 1997.
- [29] George EP Box, Gwilym M Jenkins, Gregory C Reinsel, and Greta M Ljung. *Time series analysis: forecasting and control*. John Wiley & Sons, 2015.

A Appendix A

A.1 Full Results of 4.1.1 of the main paper

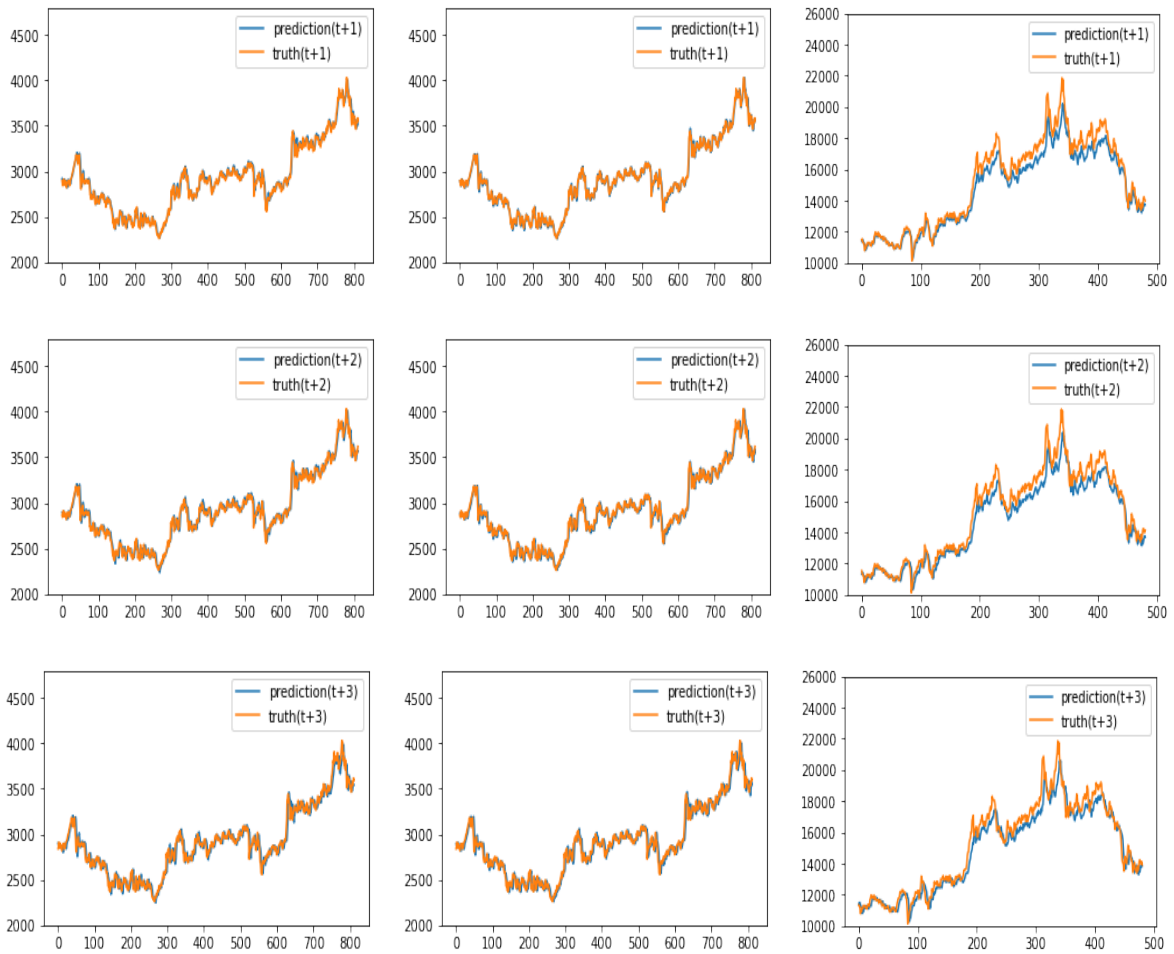


Figure 11: The prediction effect of different stocks with $\alpha = 1.5$. (left:SSE energy Index stock, middle:SSE50 Index stock, right:SSE Consumer Index stock)

A.2 Full Results of 4.1.2 of the main paper:SSE 50 Index Stock

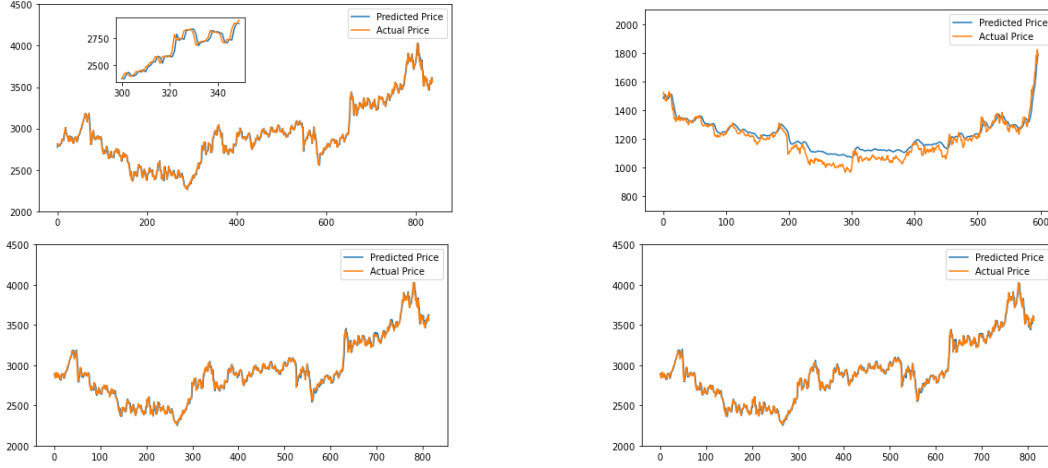


Figure 12: For SSE 50 Index stock, the predictive effects of different models. (The upper left is ARIMA, the upper right is LSTM, the lower left is SDE-Net, the lower right is LDE-Net.)

B Appendix B

In this section, we will prove the convergence rate of the neural network model constructed under the Euler discretization framework of stochastic differential equations. Among them, the drift term and diffusion term in the network structure are learned through two independent neural networks. Similar to the method used in the proof of strong convergence rate of Euler-Maruyama method in Liu [26], we consider $\{X^{(m)}(t)\}_{t \in [0, T]}$, the continuous version of Euler-Maruyama method with respect to equation (4.1):

$$X^{(m)}(t) = X^{(m)}(0) + \int_0^t f_m(\overline{X^{(m)}}(s); \theta_f) ds + g_m(X_0^{(m)}; \theta_g) L(t), \quad X^{(m)}(0) = x_0,$$

where $\overline{X^{(m)}}(t) = X_k^{(m)}$ for $t \in [k\Delta t, (k+1)\Delta t)$ is the discrete version of Euler-Maruyama method. Then, we can get the following lemma:

Lemma B.1. *Suppose that Assumption H1 holds, for every $t \in [0, T]$, the difference between $X^{(m)}$ and $\overline{X^{(m)}}$, the respectively continuous and discrete versions of the Euler-Maruyama method is*

$$\mathbb{E}|\overline{X^{(m)}}(t) - X^{(m)}(t)| \leq C_6(\Delta t)^{\frac{1}{\alpha}},$$

where C_3 is a constant dependent on index α (see the exact expression of C_3 in [27]), constant $C_4 = 3(\mathbb{E}|x_0| + 2K_1T + C_3T^{\frac{1}{\alpha}}|g_m(x_0)|)$, constant $C_5 = C_4 + e^{6K_1T}$ and constant $C_6 = 4K_1(1 + C_5) + 2|g_m(x_0)|C_3$.

Lemma B.2. *Suppose that Assumption H1 holds, the strong error of the Euler-Maruyama method (B) for equation (4.2) is*

$$\sup_{0 \leq t \leq T} \mathbb{E}|x^{(m)}(t) - X^{(m)}(t)| \leq (\Delta t)^{\frac{1}{\alpha}} KC_6T \exp(KT),$$

where $x^{(m)}$ is the solution of equation (4.2) and $X^{(m)}$ is the continuous version of the corresponding Euler-Maruyama method.

Proof.

$$\begin{aligned} |x^{(m)}(t) - X^{(m)}(t)| &= \left| \int_0^t [f_m(x^{(m)}(s)) - f_m(\overline{X^{(m)}}(s))] ds \right| \\ &= \int_0^t |f_m(x^{(m)}(s)) - f_m(X^{(m)}(s))| ds + \int_0^t |f_m(X^{(m)}(s)) - f_m(\overline{X^{(m)}}(s))| ds \\ &\leq K \int_0^t |x^{(m)}(s) - X^{(m)}(s)| ds + K \int_0^t |X^{(m)}(s) - \overline{X^{(m)}}(s)| ds. \end{aligned}$$

Taking expectations on both sides,

$$\begin{aligned}\mathbb{E}|x^{(m)}(t) - X^{(m)}(t)| &\leq K\mathbb{E}\left(\int_0^t |x^{(m)}(s) - X^{(m)}(s)|ds\right) + K\mathbb{E}\left(\int_0^t |X^{(m)}(s) - \overline{X^{(m)}}(s)|ds\right) \\ &= K\int_0^t \mathbb{E}|x^{(m)}(s) - X^{(m)}(s)|ds + K\int_0^t \mathbb{E}|X^{(m)}(s) - \overline{X^{(m)}}(s)|ds.\end{aligned}$$

By Lemma B.1, we have

$$\mathbb{E}|x^{(m)}(t) - X^{(m)}(t)| \leq K\int_0^t \mathbb{E}|x^{(m)}(s) - X^{(m)}(s)|ds + KC_6(\Delta t)^{\frac{1}{\alpha}}T.$$

Using Gronwall's inequality, we get

$$\mathbb{E}|x^{(m)}(t) - X^{(m)}(t)| \leq KC_6(\Delta t)^{\frac{1}{\alpha}}T \exp(Kt).$$

Take supreme with respect to time t on both side, we get

$$\sup_{0 \leq t \leq T} \mathbb{E}|x^{(m)}(t) - X^{(m)}(t)| \leq KC_6(\Delta t)^{\frac{1}{\alpha}}T \exp(KT).$$

□

Proof of Lemma 4.2. First, we have

$$\mathbb{E}|\overline{X^{(m)}} - x^{(m)}| \leq \mathbb{E}|\overline{X^{(m)}} - X^{(m)}| + \mathbb{E}|X^{(m)} - x^{(m)}|.$$

Then, applying Lemma B.1 and Lemma B.2, we can get

$$\begin{aligned}\sup_{0 \leq t \leq T} \mathbb{E}|\overline{X^{(m)}} - x^{(m)}| &\leq \sup_{0 \leq t \leq T} \mathbb{E}|\overline{X^{(m)}} - X^{(m)}| + \sup_{0 \leq t \leq T} \mathbb{E}|X^{(m)} - x^{(m)}| \\ &\leq (\Delta t)^{\frac{1}{\alpha}}KC_6T \exp(KT).\end{aligned}$$

□

Proof of Lemma 4.4. For all $t \in [0, T]$,

$$\begin{aligned}|x^{(m)}(t) - Y(t)| &\leq \int_0^t |f_m(x^{(m)}(s)) - f(Y(s))|ds + |(g_m - g)L_t| \\ &\leq \int_0^t |f_m(x^{(m)}(s)) - f(x^{(m)}(s))|ds + \int_0^t |f(x^{(m)}(s)) - f(Y(s))|ds + |(g_m - g)L_t|.\end{aligned}$$

Take supreme with respect to time t on both side, we get

$$\sup_{t \in [0, T]} |x^{(m)}(t) - Y(t)| \leq \int_0^t |f_m(x^{(m)}(s)) - f(x^{(m)}(s))|ds + \int_0^t |f(x^{(m)}(s)) - f(Y(s))|ds + |(g_m - g)|C,$$

where constant C is the bound of $|L_t|$. Then, take expectation on both side, we get

$$\mathbb{E}\left(\sup_{t \in [0, T]} |x^{(m)}(t) - Y(t)|\right) \leq \mathbb{E}\left(\int_0^T |f_m(x^{(m)}(s)) - f(x^{(m)}(s))|ds\right) + \mathbb{E}\left(\int_0^T |f(x^{(m)}(s)) - f(Y(s))|ds\right) + |(g_m - g)|C.$$

By Fubini Theorem and Cauchy-Schwartz inequality, we get

$$\begin{aligned}\mathbb{E}\left(\int_0^T |f_m(x^{(m)}(s)) - f(x^{(m)}(s))|ds\right) &= \int_0^T \int_{\mathbb{R}^d} |f_m(x) - f(x)|\mu_s^{(m)}(x)dxds \\ &\leq \left|\int_0^T \|f_m(x) - f(x)\|_{L^2}^2 ds\right|^{\frac{1}{2}} \cdot \left|\int_0^T \int_{\mathbb{R}^d} (\mu_s^{(m)}(x))^2 dx ds\right|^{\frac{1}{2}} \\ &\leq M^{\frac{1}{2}}T \|f_m - f\|_{L^2} \\ &\leq \frac{M^{\frac{1}{2}}TC_1}{m^{\frac{1}{2}}}.\end{aligned}$$

The last inequality is obtained via inequality (4.3). Thus,

$$\begin{aligned} \mathbb{E}(\sup_{t \in [0, T]} |x^{(m)}(t) - Y(t)|) &\leq \mathbb{E}(\int_0^T |f(x^{(m)}(s)) - f(Y(s))| ds) + \frac{M^{\frac{1}{2}}TC_1}{m^{\frac{1}{2}}} + \frac{C_2}{m^{\frac{1}{2}}}C \\ &= \mathbb{E}(\int_0^T |f(x^{(m)}(s)) - f(Y(s))| ds) + m^{-\frac{1}{2}}(M^{\frac{1}{2}}TC_1 + C_2C). \end{aligned}$$

By the Lipschitz continuity of f and Fubini's theorem,

$$\mathbb{E}(\int_0^T |f(x^{(m)}(s)) - f(Y(s))| ds) \leq L \int_0^T \mathbb{E}(\sup_{t \in [0, s]} |x^{(m)}(t) - Y(t)|) ds,$$

where L is the Lipschitz constant of f . Take $v^{(m)}(s) = \mathbb{E}(\sup_{t \in [0, s]} |x^{(m)}(t) - Y(t)|)$. We get

$$v^{(m)}(T) \leq L \int_0^T v^{(m)}(s) ds + \frac{1}{m^{\frac{1}{2}}}(M^{\frac{1}{2}}TC_1 + CC_2).$$

By Gronwall inequality, we get

$$v^{(m)}(T) \leq m^{-\frac{1}{2}}(M^{\frac{1}{2}}TC_1 + CC_2) \exp(LT),$$

that is

$$\mathbb{E}(\sup_{t \in [0, T]} |x^{(m)}(t) - Y(t)|) \leq \frac{\tilde{C}(T)}{m^{\frac{1}{2}}},$$

where we have $\tilde{C}(T) = (M^{\frac{1}{2}}TC_1 + CC_2) \exp(LT)$. □

Proof of Theorem 4.5. From Lemma 4.2 and Lemma 4.4, we can easily get:

$$\begin{aligned} \sup_{0 \leq t \leq T} \mathbb{E}|\overline{X^{(m)}}(t) - Y(t)| &= \sup_{0 \leq t \leq T} \mathbb{E}|x^{(m)}(t) - Y(t)| + \sup_{0 \leq t \leq T} \mathbb{E}|\overline{X^{(m)}}(t) - x^{(m)}(t)| \\ &\leq \mathbb{E}(\sup_{t \in [0, T]} |x^{(m)}(t) - Y(t)|) + \sup_{0 \leq t \leq T} \mathbb{E}|\overline{X^{(m)}}(t) - x^{(m)}(t)| \\ &\leq \frac{\tilde{C}(T)}{m^{\frac{1}{2}}} + (\Delta t)^{\frac{1}{\alpha}} KC_6 T \exp(KT), \end{aligned}$$

where we have $\tilde{C}(T) = (M^{\frac{1}{2}}TC_1 + CC_2) \exp(LT)$, C_3 is a constant dependent on α (see the exact expression of C_3 in [27]), $C_4 = 3(\mathbb{E}|x_0| + 2K_1T + C_3T^{\frac{1}{\alpha}}|g_m(x_0)|)$, $C_5 = C_4 + e^{6K_1T}$ and $C_6 = 4K_1(1 + C_5) + 2|g_m(x_0)|C_3$. $\overline{X^{(m)}}(t) = X_k^{(m)}$ for $t \in [k\Delta t, (k+1)\Delta t)$. □